JAMES | Journal of Advances in Modeling Earth Systems®

RESEARCH ARTICLE
10.1029/2022MS003285

Special Section:
Using radiative-convective equilibrium to understand convective organization, clouds, and tropical climate

Three Rules for the Decrease of Tropical Convection With Global Warming

Nadir Jeevanjee[1]

[1]Geophysical Fluid Dynamics Laboratory, Princeton, NJ, USA

Key Points:

- Three constraints on tropical convection can all be derived analytically from clear-sky subsidence
- Tropospheric mass fluxes at a fixed isotherm should robustly decrease under global warming
- Decreases in anvil cloud area and cloud-base mass flux are not as robust

Correspondence to:
N. Jeevanjee,
nadir.jeevanjee@noaa.gov

Citation:
Jeevanjee, N. (2022). Three rules for the decrease of tropical convection with global warming. *Journal of Advances in Modeling Earth Systems*, *14*, e2022MS003285. https://doi.org/10.1029/2022MS003285

Received 3 JUL 2022
Accepted 7 OCT 2022
Corrected 10 APR 2023

This article was corrected on 10 APR 2023. See the end of the full text for details.

Abstract Tropical convection is expected to decrease with warming, in a variety of ways. Specific incarnations of this idea include the "stability-iris" hypothesis of decreasing anvil cloud coverage, as well as the decrease of both tropospheric and cloud-base mass fluxes with warming. This paper seeks to encapsulate these phenomena into three "rules," and to explore their interrelationships and robustness, using both analytical reasoning as well as cloud-resolving and global climate simulations. We find that each of these rules can be derived analytically from the usual expression for clear-sky subsidence, so they all embody the same essential physics. But, these rules do not all provide the same degree of constraint: the stability-iris effect is not entirely robust due to unconstrained microphysical degrees of freedom, and the decrease in cloud-base mass flux is not entirely robust due to unconstrained effects of entrainment and detrainment. Tropospheric mass fluxes on the other hand are shown to be well-constrained theoretically, and when evaluated in temperature coordinates they exhibit a monotonic decrease with warming at all vertical levels and across a hierarchy of models.

Plain Language Summary Tropical convection and high cloudiness are expected to decrease with global warming, in a variety of ways. This phenomenon has a few different manifestations in the literature, whose relationships are unclear. We show analytically that these explanations all embody the same essential physics, but are not equally robust and thus do not all have the same predictive power.

1. Introduction

There is a sense in the literature that tropical convection should "decrease" with global warming, in various ways. Perhaps the earliest incarnation of this idea is the reduction in the tropical overturning circulation first hypothesized by A. K. Betts and Ridgway (1989), and later demonstrated in global climate models (e.g., Knutson & Manabe, 1995; Vecchi & Soden, 2007). Another, seemingly related manifestation of this idea is that cloud-base convective mass fluxes should decrease with warming, again first noted by Betts (A. Betts, 1998), and later reiterated by Held and Soden (2006). Chadwick et al. (2013) and Jenney et al. (2020) then found a weakening of convective mass fluxes *throughout* the troposphere, potentially generalizing these earlier results. Finally, Bony et al. (2016) argued via moist thermodynamics and mass conservation that tropical anvil cloud areas should decrease with warming, an argument known as the "stability-iris" hypothesis. Bony et al. (2016) found evidence for the stability-iris in GCMs, with further evidence found in observations (Ito & Masunaga, 2022; Saint-Lu et al., 2020, 2022) as well as cloud-resolving models (Beydoun et al., 2021; Cronin & Wing, 2017).

A lingering question about all these phenomena, however, is the degree to which they are related. Are they all equivalent somehow, or do their underlying physics differ? For example, the weakening of the tropical circulation and the decrease in tropospheric convective mass flux are governed by changes in the clear-sky subsidence velocity [Equation 1 below], whereas the decrease in *cloud-base* mass flux is governed by the bulk atmospheric water/energy budget [Equation 6 below]. These constraints look different superficially, but at the same time both ultimately depend on the difference in how atmospheric radiative cooling and atmospheric moisture scale with global warming. This suggests a potential equivalence between the mechanisms, which has not been pursued or made precise.

Beyond equivalence, there is also the question of whether these phenomena are equally robust. While decreases in circulation strength and convective mass flux with warming seem to occur with few exceptions, the same is not true of the stability-iris effect: some earlier studies with cloud-resolving models found an *increase* of anvil cloud area with warming (Singh & O'Gorman, 2015; Tsushima et al., 2014), with the more recent RCEMIP intercomparison finding a similar increase in roughly 1/3 of participating models (Stauffer & Wing, 2022; Wing et al., 2020). This diversity amongst models leads to a correspondingly large uncertainty in the associated

"tropical anvil cloud area feedback," whose magnitude and uncertainty range rival those of all other cloud feedbacks (Sherwood et al., 2020).

Given this state of affairs, it seems worthwhile to more closely scrutinize these different manifestations of decreasing convection, assessing both their inter-relatedness and robustness. We attempt this here by encapsulating these phenomena into three "rules," showing mathematically that they are indeed closely related, and in some cases equivalent. In fact, all three phenomena spring from a common origin, namely the well-known expression [Equation 1 below] for subsidence vertical velocity. The specific mathematical forms of these rules suggest varying degrees of robustness, however, which we evaluate with both global and cloud-resolving simulations.

We focus here on the stability-iris effect (Section 2) and the decrease of convective mass fluxes both throughout the troposphere and at cloud base (Sections 3 and 4). The implications of these phenomena for the large-scale circulation are important and require a paper in their own right; some discussion of the relevant issues is given in the conclusions. The simulations utilized here are primarily cloud-resolving simulations performed with GFDL's FV^3 dynamical core, run in doubly periodic radiative-convective equilibrium (RCE) over a range of surface temperatures with non-interactive radiation and a simplified, warm-rain only microphysics scheme. These idealized simulations are supplemented by more comprehensive cloud-resolving simulations with DAM (Romps, 2008), which include full complexity microphysics as well as interactive radiation. We also test some of our conclusions using 1pct_CO2 GCM simulations conducted with GFDL's CM4 (Held et al., 2019). All diagnostics reported here are time and domain mean unless otherwise stated. Further details of both sets of cloud-resolving simulations are given in the Appendices.

1.1. Subsidence Vertical Velocity

The expression for the subsidence vertical velocity is derived (e.g., Jenney et al., 2020) by considering the thermodynamic energy equation in regions where there is no condensation heating (such regions are typically clear-sky, but can also include cloudy, non-ascending regions such as anvil clouds). The only diabatic heat sources are then radiative and evaporative cooling, denoted $\mathcal{H}_{\text{rad}}$ and $\mathcal{H}_{\text{e}}$ respectively, both negative and in units of K/s. Neglecting horizontal heat transport, the thermodynamic energy equation then implies that the steady-state "clear-sky" subsidence velocity $w_{\text{sub}} < 0$ is given by

$$w_{\text{sub}} = \frac{\mathcal{H}_{\text{rad}} + \mathcal{H}_{\text{e}}}{\Gamma_d - \Gamma}. \tag{1}$$

Here Γ_d and Γ have their usual meanings as the dry and actual lapse rates, respectively. The difference $\Gamma_d - \Gamma$ is of course due to the presence of moisture, in a sense we will make precise below, so the Equation 1 indeed combines information about radiation and moisture. Equation 1 will be the starting point for each of our rules going forward. Note that evaporative cooling $\mathcal{H}_{\text{e}}$ is often neglected in calculations of w_{sub} (e.g., Bony et al., 2016), despite the fact that precipitation efficiencies can be 0.5 or less and hence $\mathcal{H}_{\text{e}}$ is often equal to or greater than $\mathcal{H}_{\text{rad}}$ (Jeevanjee & Zhou, 2022; Lutsko et al., 2021).

2. Stability-Iris

We begin with the stability-iris hypothesis of Bony et al. (2016). The subsidence vertical velocity in Equation 1 is not uniform in the vertical, and thus has a nonzero divergence which must be balanced by a horizontal clear-sky convergence CSC $= \partial_z w_{\text{sub}}$, or

$$\text{CSC} = \partial_z \left(\frac{\mathcal{H}_{\text{rad}} + \mathcal{H}_{\text{e}}}{\Gamma_d - \Gamma} \right) \tag{2}$$

(in invoking mass continuity here we neglect vertical variations in density). This horizontal convergence into clear-skies must be balanced by net convective detrainment (or divergence) from cloudy skies, so the above is also an expression for net convective detrainment. The stability-iris hypothesis argues that because moist adiabatic lapse rates decrease at a fixed isotherm with surface warming (Figure A1a), then the denominator in Equation 2 should increase with warming, and hence CSC should decrease (this decrease in the denominator dominates over changes in radiative cooling in the numerator; Knutson & Manabe, 1995; Bony et al., 2016). The stability-iris hypothesis further assumes that cloud fraction is in some sense proportional to net convective detrainment, a key

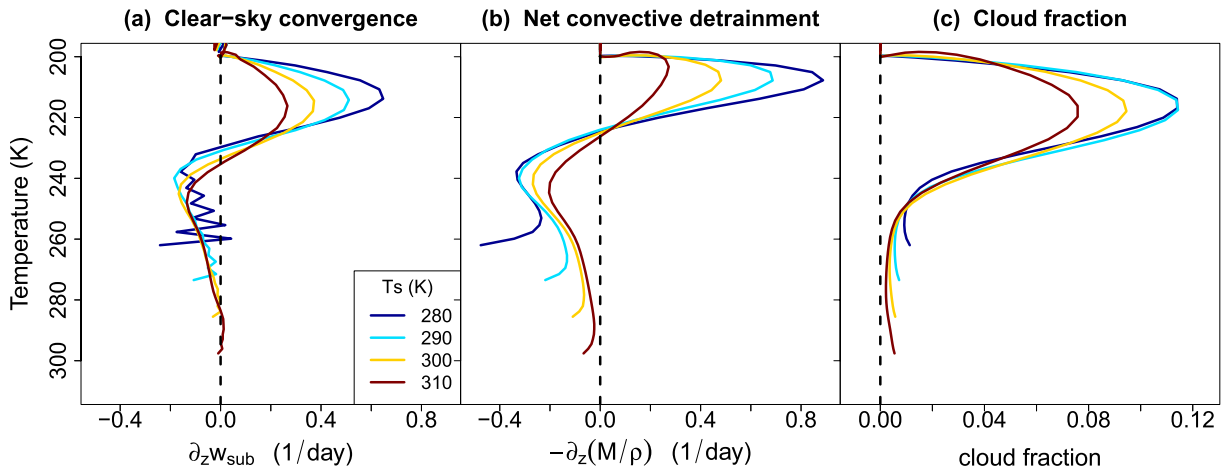

Figure 1. *Simulations results are consistent with the stability-iris hypothesis, but the relationship between CSC/detrainment and cloud fraction is not proportional.* Shown here are simulated profiles of (a) clear-sky convergence as diagnosed via Equation 2 (b) convective detrainment $-\partial_z(M/\rho)$ where the convective mass flux M is diagnosed as described in Appendix A, and (c) cloud fraction. Panels (a and b) are similar, as required by mass continuity, and all three panels show a decrease in their upper-tropospheric maxima with warming. But the CSC and detrainment profiles are not sign-definite, whereas cloud fraction is. Here and elsewhere profiles are cut off at cloud base for clarity.

assumption which we dwell on below. Combining these arguments for the moment, we then have our first rule for how convection decreases under global warming:

Rule 1. (Stability-iris): Clear-sky convergence, net convective detrainment, and anvil cloudiness should decrease together with warming.

Figure 1 tests this rule by showing profiles of cloud fraction (diagnosed as the fraction of grid cells with condensate mixing ratios greater than 10^{-5}), CSC [diagnosed via Equation 2], and net convective detrainment $-\partial_z(M/\rho)$ (where M is the convective mass flux diagnosed via conditional sampling of convecting grid cells, in kg/m^2/s; see Appendix A for details). These profiles are all drawn from our FV^3 RCE simulations, using temperature as a vertical coordinate since CSC and anvil cloud peaks are well known to follow isotherms much more closely than isobars under global warming (i.e., the "Fixed Anvil Temperature" hypothesis, Hartmann & Larson, 2002; Hartmann et al., 2019). Figures 1a and 1b explicitly confirm, for the first time to our knowledge, that the independently diagnosed profiles of clear-sky convergence and net convective detrainment are roughly the same (as they should be by mass continuity). Furthermore, these profiles both show a decrease in their upper-level maxima with warming, as do the cloud fraction profiles in panel c. These results are all consistent with Rule 1 above.

But, Figure 1 does not show a straightforward proportionality between CSC/detrainment and cloud fraction; to the contrary, the CSC/detrainment profiles actually *change sign* in the vertical, as net entrainment in the lower troposphere gives way to net detrainment in the upper troposphere. The cloud fraction profiles are meanwhile positive definite, so the relationship between CSC/detrainment and cloud fraction cannot be a direct proportionality. Indeed, a more complex relationship was recently derived by Beydoun et al. (2021), who showed that to first order, cloud fraction C can be related to CSC as

$$C = \mathrm{CSC} \cdot \Delta_h l \cdot \tau \tag{3}$$

where $\Delta_h l$ is a horizontal finite-difference in log cloud condensate across the anvils, and τ is an inverted sum of microphysical and vertical advection time tendencies for log cloud condensate. This relationship shows that cloud fraction is determined not only by CSC, which must obey Equation 2, but also by microphysical degrees of freedom which are largely unconstrained. Indeed, these extra degrees of freedom explain how CSC can change sign, yet still be tied via Equation 3 to positive-definite cloud fraction; all that is needed is an accompanying sign change in τ. Such a sign change might even be anticipated, as microphysical processes transition from being a source of cloud condensate in the lower troposphere (via condensation) to a sink in the upper troposphere (via sedimentation).

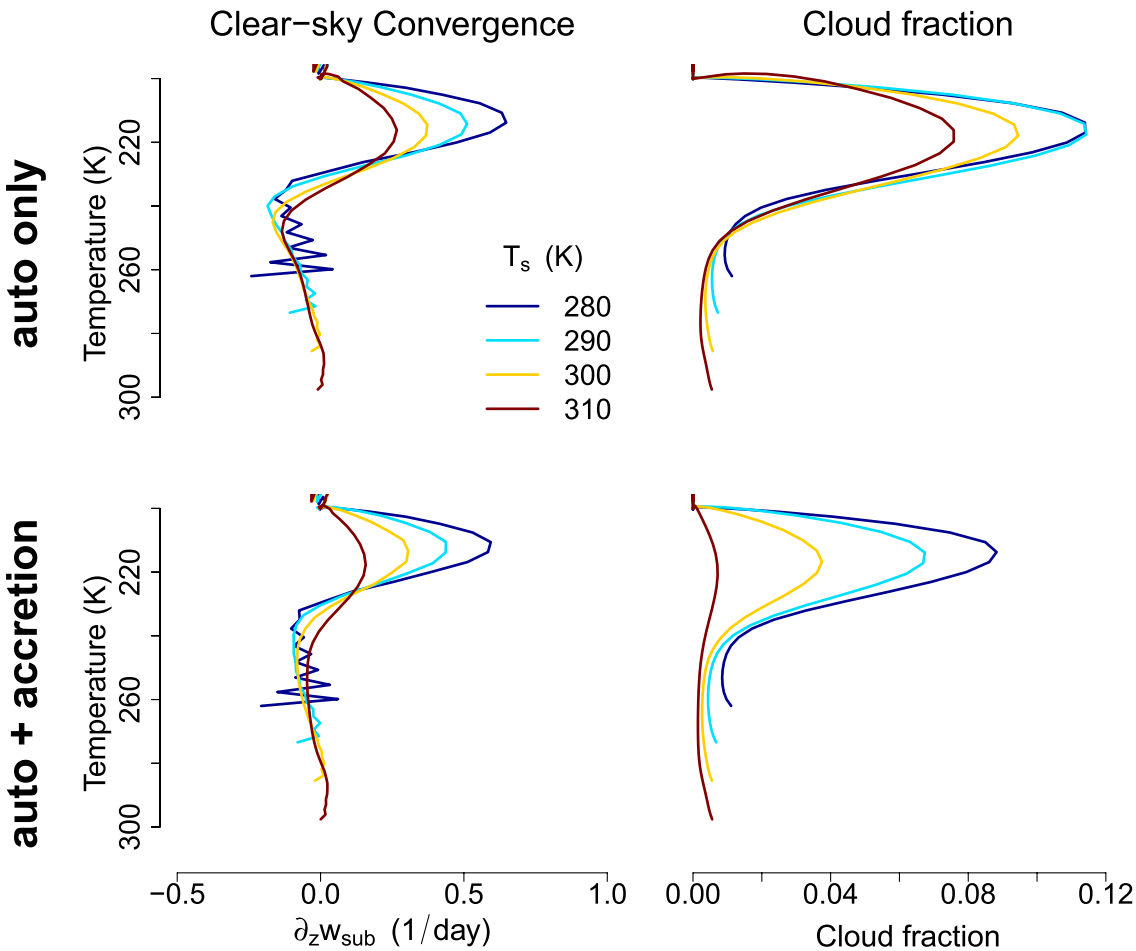

Figure 2. *Similar CSC peaks do not necessarily imply similar anvil cloud fractions*. The top row reproduces the CSC and cloud profiles from Figure 1, whereas the bottom row shows analogous results from simulations run with warm-rain accretion on. Profiles are again cut off at cloud base for clarity.

To emphasize that the microphysical degrees of freedom in Equation 3 prevent a 1-1 relationship between cloud fraction and CSC, we re-run our simulations with not only warm-rain autconversion (the default setting) but also an additional, widely used accretion process which converts cloud condensate to rain (Y.-L. Lin et al., 1983, Equation 51). Profiles of CSC and cloud fraction from these simulations are shown in Figure 2. These profiles demonstrate explicitly that similar CSC profiles do not imply similar cloud fraction profiles.

These results suggest that even if CSC is a leading-order control on cloud fraction, the presence of largely unconstrained microphysical degrees of freedom limits the predictive power of Equation 3. In particular, CSC decreases with warming might *typically* lead to anvil area decreases with warming, but this is not guaranteed to be the case. This is consistent with the aforementioned RCEMIP result that roughly 2/3 of models exhibit a stability iris-effect, but 1/3 do not. Similarly, Beydoun et al. (2021) found an overall stability-iris effect in analyzing RCE simulations over a large SST range, but found the connection between CSC and anvil area to be non-monotonic *within* their SST range. These results from the literature, along with the results shown here, suggest that Rule 1 is a general tendency of models, but is not entirely robust.

Another formalism for cloud fraction was introduced by Seeley et al. (2019, hereafter S19), who expressed cloud fraction as a product of *gross* detrainment and a positive-definite cloud lifetime. Gross detrainment is not as easily constrained as net detrainment/CSC, but S19's cloud lifetime can be more simply interpreted as a positive-definite lifetime of detrained cloud condensate. Regardless of these differences, however, the implication of the S19 formalism is similar: microphysical timescales play a leading-order role along with detrainment, so changes in detrainment alone may be insufficient to predict changes in anvil area.

3. Mass Flux Profiles

One can obtain another view of decreasing convection with warming by again beginning with Equation 1 and noting that w_{sub} should decrease with warming throughout the troposphere due to the thermodynamically constrained increase in the denominator (Knutson & Manabe, 1995). Invoking the fact that the convective mass flux M must be equal and opposite to the subsidence mass flux ρw_{sub} (assuming the subsidence area fraction is very close to 1), this then also implies that *convective mass fluxes should decrease throughout the troposphere with warming*. This is a straightforward consequence of the arguments of Knutson and Manabe (1995), but has not been emphasized in the literature and has only been sporadically studied (Chadwick et al., 2013; Jenney et al., 2020).

Before formalizing this rule and testing it here, we make it somewhat more precise by rewriting w_{sub} in a more convenient form. We first rewrite $\mathcal{H}_{rad} = \frac{g}{C_p}\partial_p F$ (where F is the net upward radiative flux) and $\mathcal{H}_e = -Le/\rho C_p$, where e (and later c) is the domain-mean evaporation (condensation) in kg/m^3/s. Then multiplying the numerator and denominator in Equation 1 by C_p/Γ and applying the chain rule, we obtain after some manipulation

$$M = -\rho w_{sub} = \frac{-\partial_T F + \frac{Le}{\Gamma}}{g\left(\frac{1}{\Gamma} - \frac{1}{\Gamma_d}\right)}. \tag{4}$$

Next we note that by local energy balance we have $L(c - e) = \partial_z F$ [see also Equation 10 below], and we also define a local "conversion efficiency" $\alpha \equiv (c - e)/c$. Combining these relations, one can rewrite Equation 4 as

$$M = \frac{1}{\alpha}\frac{-\partial_T F}{g\left(\frac{1}{\Gamma} - \frac{1}{\Gamma_d}\right)}. \tag{5}$$

The advantage of this form is that if we use temperature as a vertical coordinate, the numerator becomes tightly constrained: Jeevanjee and Romps (2018) showed, on both theoretical grounds and with cloud-resolving RCE simulations, that the profile $(-\partial_T F)(T)$ is "T_s-invariant," that is, the profile does not depend on T_s (this was also shown across cloud-resolving models in Stauffer & Wing, 2022). In contrast, the factor of $(1/\Gamma - 1/\Gamma_d)^{-1}$ is quite sensitive to T_s; indeed its upper-tropospheric peak near $T = 220$ K decreases at almost a halving for every 10 K of surface warming, approximately equal to Clausius-Clapeyron scaling (Figure A1b). Thus, barring significant changes in the conversion efficiency α (which we do not find, Figure A1c), we expect the stability-related decreases in $(1/\Gamma - 1/\Gamma_d)^{-1}$ with warming to dominate changes at a given isotherm, hence:

Rule 2. Convective mass flux profiles $M(T)$ should decrease at all isotherms with surface warming.

This prediction of Equation 5 is confirmed for our simulations in Figure 3a, for both the subsidence mass flux $-\rho w_{sub}$ diagnosed via Equation 1 as well as the conditionally sampled convective mass flux M. Similarly to Figure 1, this panel confirms the equality of M and -ρw_{sub}, and thus confirms that the latter can be used to constrain the former (slight discrepancies between the two may be explained by the sensitivity of M to the thresholds used in its diagnosis—Appendix A). As per Rule 2, the profiles in Figure 3a are plotted in temperature coordinates, in which they exhibit a clean decrease with warming at essentially all levels (profiles are, however, cut-off near cloud base for clarity; the behavior of cloud-base M is discussed in the next section). Figure 3b, plotted in pressure coordinate, shows on the other hand that on isobars, the decrease of M and ρw_{sub} with warming fails in the upper troposphere. Thus, the decrease of upper-tropospheric M with warming depends on the choice of vertical coordinate.

The strong theoretical foundation and encouraging validation of Rule 2 make it a candidate for a robust response of tropical convection to global warming. But, this validation has so far only taken place in the context of an idealized, limited-area cloud-resolving model, so further validation across the model hierarchy is required (Jeevanjee et al., 2017). To this end, we first reproduce Figures 3a and 3b but using DAM simulations; the results are shown in Figures 3c and 3d. These simulations feature interactive radiation and comprehensive microphysics, yet still show a clean decrease of M at virtually all isotherms (Figure 3c), again in contrast to the picture in pressure coordinates (Figure 3d). The rough equality of M and ρw_{sub} is also evident.

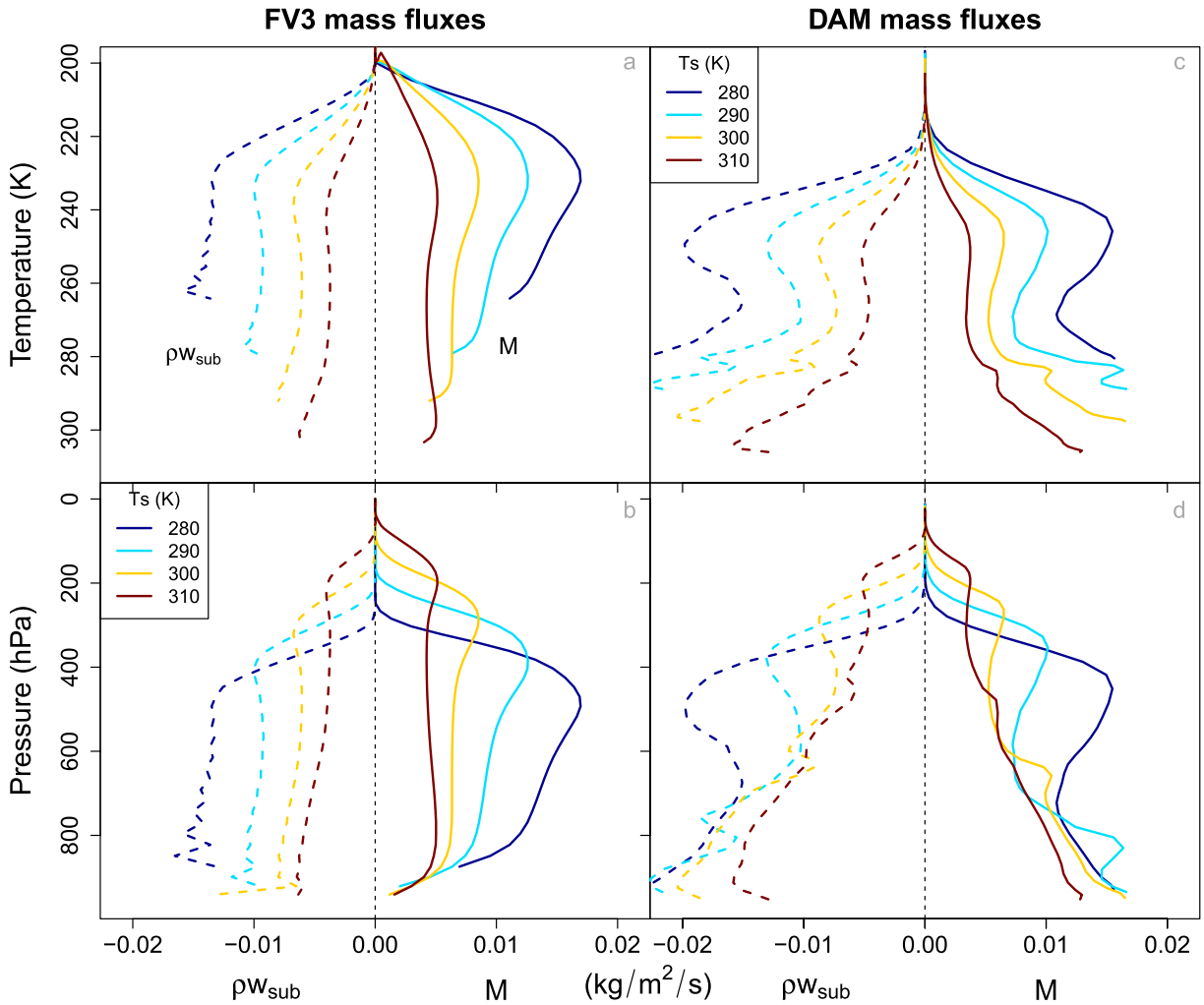

Figure 3. *Mass fluxes decrease with warming throughout the free troposphere, most robustly when plotted in temperature coordinates*. (a) shows that both (minus) the subsidence mass flux $-\rho w_{sub}$ and the convective mass flux M, which are independently diagnosed, decrease at essentially all isotherms due to surface warming. This decrease is not evident in the upper troposphere when pressure coordinates are used (panel b). (c and d) show analogous results, but from higher complexity Das Atmosphärische Modell simulations.

Next, we validate Rule 2 in a GCM. We use a 1pct_CO2 run of GFDL's CMIP6-generation coupled model CM4, from which monthly mean parameterized convective mass flux profiles M_c were saved (see Zhao et al., 2018, for details of CM4's "double-plume" convective parameterization). Figure 4 shows a map of time-averaged M_c evaluated at 850 hPa, as well as tropical mean (20°S–20°N) profiles averaged in both pressure and temperature coordinates over years 1–20, 60–80, and 130–150. The map shows the marked spatial heterogeneity of M_c, similar to the pattern of tropical rainfall. Despite this complexity, however, the tropical mean profiles behave similarly to those from our RCE simulations: M_c decreases with warming throughout the troposphere, and this decrease occurs at all levels in temperature coordinates but not in pressure coordinates. In fact, the insets show that in the upper troposphere, the use of pressure coordinates actually *changes the sign* of the M_c response to warming, further underscoring the importance of the choice of vertical coordinate.

The fact that upper tropospheric M (on fixed isotherms) decreases robustly with warming can actually be seen as the basis for Rule 1: if we know that upper-tropospheric mass fluxes decrease, then it follows fairly naturally that their detrainment should also decrease. Indeed, the changes in stability which drive the decrease in M [cf. Equation 5] are the same changes which are thought to drive the changes in the CSC peak under the stability-iris hypothesis (Section 2).

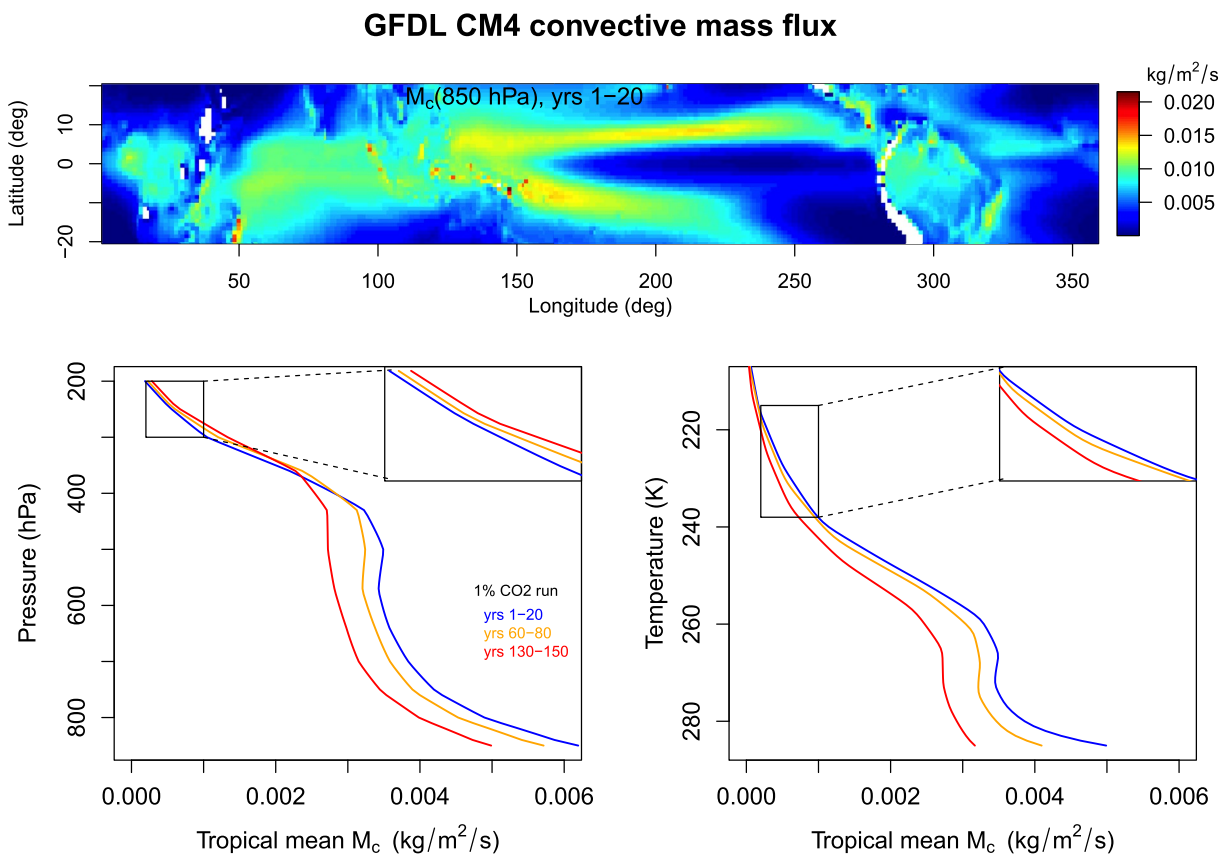

Figure 4. *Tropical-mean mass fluxes from a GCM behave similarly to the RCE results*. This figure shows the parameterized convective mass flux M_c from a 1%CO_2 run of GFDL's CM4 coupled model. The top panel shows a map of M_c(850 hPa) averaged over years 1–20 of the simulation, while the bottom panels show tropical mean (20°S - 20°N) profiles averaged in both pressure and temperature coordinates over years 1–20, 60–80, and 130–150. Despite the complexity evident in the top panel, the tropical mean M_c profiles also decrease robustly throughout the free troposphere, particularly when plotted in temperature coordinates. The insets in the bottom panels show that the *sign* of the mass flux change depends on the choice of vertical coordinate.

4. Cloud-Base Mass Flux

A third perspective on decreasing convection with warming, popularized by Held and Soden (2006) and stemming from a slightly different formulation in A. Betts (1998, see Appendix C), begins by noting that the cloud-base (or lifting condensation level) convective latent heat flux should equal the mean precipitation, or equivalently the column-integrated free tropospheric radiative cooling Q_{ft} (W/m^2). Mathematically, this is expressed as

$$(Lq_v^* M)|_{\text{LCL}} = Q_{\text{ft}}. \tag{6}$$

From this it follows that the cloud-base mass flux $M|_{\text{LCL}}$ should decrease with warming, because Q_{ft} increases by 1%–3%/K (e.g., Jeevanjee & Romps, 2018) whereas $q_v^*|_{\text{LCL}}$ increases by 7%/K. We thus obtain a third rule, which we refer to as "Betts's rule":

Rule 3. **(Betts's rule)**: Cloud-base convective mass fluxes $M|_{\text{LCL}}$ should decrease with surface warming.

This rule was confirmed in a particular GCM by Held and Soden (2006) (although they used mass fluxes evaluated at 500 hPa rather than cloud-base). On the other hand, Schneider et al. (2010) also evaluated the accuracy of Equation 6 (their Equation 8b), and found only middling agreement with their GCM simulations. Here, we can make a quick and qualitative evaluation using the mass flux profiles already shown: the FV^3 profiles in Figure 3b seem consistent with Betts's rule, but the DAM profiles in Figure 3d do not, instead exhibiting non-monotonic changes in M with warming below 800 hPa or so.

These mixed results suggest that Betts's rule is not robust. But, how can the simple argument leading to Equation 6 fail? And how does Betts's rule connect to our previous rules? We argue here that Betts's rule may not be

robust because it assumes that all water vapor lofted above cloud-base both condenses and precipitates to the surface. In other words, Equation 6 ignores detrainment (and entrainment) of water vapor, and also assumes unit precipitation efficiency. We will analytically derive a generalization of Betts's rule from our fundamental Equation 1 which accounts for these effects, and show that the associated terms are poorly constrained and plausibly lead to the behavior seen in Figure 3.

We begin by rewriting Equation 1 in terms of a flux divergence in z coordinates:

$$M = \frac{\partial_z F + Le}{C_p(\Gamma_d - \Gamma)}. \tag{7}$$

Next, we note that for a saturated, convecting parcel experiencing fractional entrainment per unit distance ϵ (m^{-1}), its saturated moist static energy (MSE) h^* evolves as (Singh & O'Gorman, 2013)

$$\partial_z h^* = -\epsilon(1 - \mathrm{RH}) L q_v^*. \tag{8}$$

This expression captures the dilution of MSE by mixing with subsaturated environmental air. Using the definition $h^* = C_p T + gz + Lq_v^*$, and with some manipulation, this can be re-written as

$$C_p(\Gamma_d - \Gamma) = \underbrace{L\left[-\frac{dq_v^*}{dz} - \epsilon(1 - \mathrm{RH}) q_v^*\right]}_{c/M}. \tag{9}$$

This equation has lapse rates on one side and terms involving q_v^* on the other, thus yielding the promised connection between moisture and stability. Furthermore, bulk-plume models of the atmosphere show that the domain-mean condensation rate $c = M[-\partial_z q_v^* - \epsilon(1 - \mathrm{RH}) q_v^*]$ (for example, Equation 13 of Romps (2014)), and thus the right-hand side of Equation 9 is simply Lc/M. Since the difference $\Gamma_d - \Gamma$ from the left-hand side of Equation 9 also appears in Equation 7, we may substituting and rearrange, recovering our statement of local energy balance

$$\partial_z F = L(c - e). \tag{10}$$

If we now define the precipitation efficiency PE as the ratio of vertically integrated net condensation to gross condensation, then c and e are related to the precipitation efficiency as

$$PE = \frac{\int (c - e) dz}{\int c dz}. \tag{11}$$

Thus, integrating Equation 10 over the free troposphere, that is, from the lifting condensation level z_{LCL} to the tropopause height z_{tp}, and noting that $\int_{z_{\mathrm{LCL}}}^{z_{\mathrm{tp}}} \partial_z F dz = Q_{\mathrm{ft}}$, we obtain

$$Q_{\mathrm{ft}} = L \int_{z_{\mathrm{LCL}}}^{z_{\mathrm{tp}}} (c - e)\, dz = L\,\mathrm{PE} \int_{z_{\mathrm{LCL}}}^{z_{\mathrm{tp}}} c dz = L\,\mathrm{PE} \int_{z_{\mathrm{LCL}}}^{z_{\mathrm{tp}}} \left(-M \frac{dq_v^*}{dz} - \epsilon M (1 - \mathrm{RH}) q_v^*\right) dz.$$

The key step is to now integrate by parts on the right-hand side of this equation. Neglecting $q_v^*(z_{\mathrm{tp}})$ eliminates one of the boundary terms, and invoking $\partial_z M = \epsilon M - \delta M$ where δ is gross (not net) fractional detrainment then yields finally

$$(L q_v^* \mathrm{PE} M)|_{\mathrm{LCL}} + \underbrace{L\,\mathrm{PE} \int_{z_{\mathrm{LCL}}}^{z_{\mathrm{tp}}} [-\delta M + \epsilon M \mathrm{RH}] q_v^* dz}_{\text{entrainment/detrainmentterm}} = Q_{\mathrm{ft}}. \tag{12}$$

Note that the key term $(Lq_v^* \mathrm{PE}\, M)|_{\mathrm{LCL}}$ arises as a boundary term from the integration by parts. Equation 12 is the generalization of Equation 6 we seek: it accounts for non-unit precipitation efficiency, and through the "entrainment/detrainment" term accounts for possible changes in the moisture flux due to entrainment/detrainment of water vapor in the free troposphere. Equation 12 is thus more complete than Equation 6, but also potentially much less robust, particularly due to the entrainment/detrainment term which seems difficult to constrain theoretically. Indeed comparison of the FV^3 mass-flux profiles in Figures 3a and 3b, which tend to increase some-

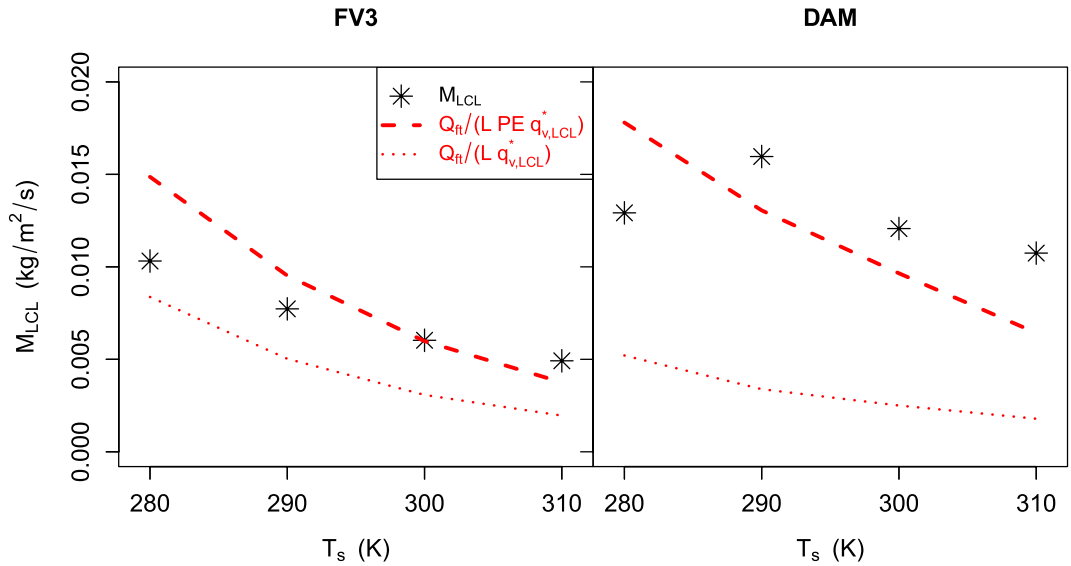

Figure 5. *Cloud-base mass fluxes do not closely follow the constraint Equation 13.* These panels show cloud-bass mass fluxes $M|_{LCL}$ plotted against surface temperature T_s, for both our FV^3 and Das Atmosphärische Modell (DAM) simulations. Markers denote $M|_{LCL}$ diagnosed directly from simulations, whereas red dashed and dotted lines denote estimates obtained from Equation 13 and Equation 6, respectively. The non-unit PE in Equation 13 yields more accurate estimates overall, but the predicted slope is too steep in FV^3 and does not capture the non-monotonicity of $M|_{LCL}$ in DAM.

what with height through the lower-mid troposphere, to the DAM mass-flux profiles in Figures 3c and 3d, which tend to decrease with height rather markedly below the freezing point, suggests that entrainment and detrainment even in RCE are not easily constrained.

One might hold out hope, however, that the entrainment/detrainment term might be negligible compared to the cloud-base term; if true, this would yield a more viable constraint of

$$(Lq_v^* \mathrm{PE}\, M)|_{LCL} \approx Q_{ft}. \tag{13}$$

We wish to test how well this version of Equation 6, which differs only by accounting for $PE \neq 1$, can predict changes in $M|_{LCL}$ with warming. This will require diagnosis of all factors in Equation 13 besides $M|_{LCL}$, from both our FV^3 and DAM simulations. We diagnose $M|_{LCL}$ as an average of M between 800 and 850 hPa, diagnose $q_v^*|_{LCL}$ as q_v at the 2nd lowest model level (this is characteristic of the boundary-layer values and thus of saturated parcels at cloud-base), diagnose Q_{ft} as the radiative cooling integrated from cloud-base to the tropopause, and diagnose precipitation efficiency according to Equation 11.

With these diagnostics in hand, Figure 5 compares the directly diagnosed $M|_{LCL}$ to $M|_{LCL}$ as estimated from both Equation 13 and Equation 6 by solving for $M|_{LCL}$. Consistent with the results of Schneider et al. (2010), this figure shows that while the theoretical estimates gives reasonable ballpark values for $M|_{LCL}$, especially when non-unit PE is accounted for, they predict a decreasing trend which is only very roughly obeyed by the models. FV^3 does show a decreasing trend, but its slope is less than half of that estimated from Equation 13. Meanwhile DAM shows a non-monotonic change of $M|_{LCL}$ with T_s, as indicated earlier. Thus, the entrainment/detrainment terms in Equation 12 seem to play a non-negligible role in the change of $M|_{LCL}$ with warming, inhibiting the robustness of Betts's rule. Inclusion of PE helps obtain more accurate values overall, but *changes* in PE with warming are small (varying between 0.56 and 0.51 in FV^3, and 0.26–0.3 in DAM) and thus do not impact the response of $M|_{LCL}$.

It is worth noting that in the original formulation of A. Betts (1998), the constraint on $M|_{LCL}$ is formulated with an additional RH-dependent term. This RH term captures the effects of entrainment/detrainment discussed above, as well as that of non-unit precipitation efficiency, but is similarly difficult to constrain. This formulation of Betts's rule is derived and discussed further in Appendix C.

Table 1
Summary of the Three Rules and Their Corresponding Constraints

Rule	Constraint
(Stability-iris) Clear-sky convergence, convective detrainment, and anvil cloud fraction decrease together with warming	$\mathrm{CSC} = \partial_z\left(\frac{\mathcal{H}_{\mathrm{rad}}+\mathcal{H}_{\mathrm{e}}}{\Gamma_d-\Gamma}\right)$
Convective mass fluxes decrease at all isotherms with surface warming	$M = \frac{1}{\alpha}\frac{-\partial_T F}{g\left(\frac{1}{\Gamma}-\frac{1}{\Gamma_d}\right)}$
(Betts's rule) Cloud-base convective mass fluxes decrease with surface warming	$(Lq_{\mathrm{v}}^{*}\mathrm{PE}M)\vert_{\mathrm{LCL}} \approx Q_{\mathrm{ft}}$

5. Summary and Discussion

This paper has shown that.

- Three rules for the decrease of convection with warming can be formulated, each of which spring from Equation 1 and thus embody the same physics
- The stability-iris effect is not entirely robust because clear-sky convergence and cloud fraction are not directly proportional, but rather are connected by loosely constrained microphysical process [Equation 3 and Figures 1 and 2]
- The decrease in tropospheric mass flux on isotherms (Rule 2) does seem to be potentially robust, based on its theoretical foundation as well as validation across a hierarchy of models [Equation 5 and Figures 3 and 4]
- Betts's rule is not entirely robust, due to the loosely constrained effects of entrainment and detrainment [Equation 12 and Figure 5].

Our three rules, along with the analytical constraints from which they are deduced, are summarized in Table 1 and illustrated schematically in Figure 6. As depicted in the schematic, the three constraints are all related to Equation 1 and each other by integration/differentiation: Equation 2 is obtained by differentiation of Equation 1, Equation 5 is simply a re-arrangement of Equation 1, and Equation 13 is obtained from Equation 1 via integration by parts.

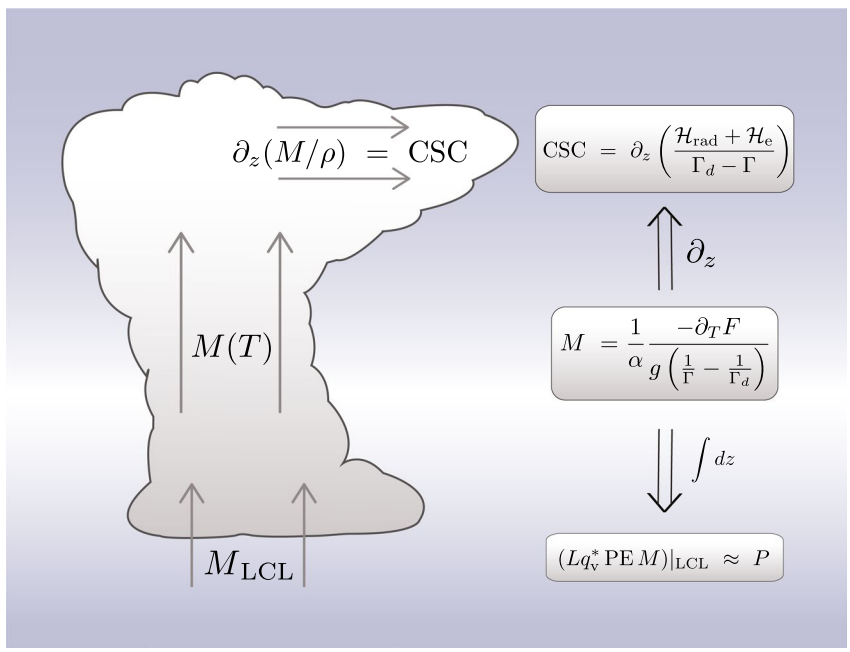

Figure 6. *The three rules pertain to the convective mass fluxes at different vertical levels, and are governed by related constraints*. The schematic pictorially depicts the three quantities of interest: divergence of upper-tropospheric mass flux $\partial_z(M/\rho) = \mathrm{CSC}$, profiles of tropospheric mass flux $M(T)$, and cloud base mass flux $M\vert_{\mathrm{LCL}}$. Also shown are the corresponding constraints and their inter-relationships via differentiation and integration.

What are the broader implications of these findings? The lack of robustness of the stability-iris hypothesis as a potential mechanism for the tropical anvil cloud area feedback has been noted before (Sherwood et al., 2020). But, our emphasis on the microphysical degrees of freedom suggests that uncertainties in this feedback may not be easily remedied, as microphysical complexity is daunting (e.g., figure 1 of Morrison et al., 2020) and high clouds appear to be sensitive to many aspects of this complexity (e.g., evolution of various ice species, sedimentation, sub-grid scale saturation adjustment; Ohno & Satoh, 2018; Ohno et al., 2020, 2021).

As for the decrease of mass flux profiles with warming: this is a straightforward consequence of decreasing w_{sub} with warming, which is well-known, but has not been emphasized in the literature. Here, we have also emphasized the importance of temperature coordinates, and leveraged the T_s-invariance of $\partial_T F$ to put the decrease of M on a stronger theoretical footing [Equation 5]. We have also confirmed that domain-mean $M = \rho w_{\text{sub}}$ in cloud-resolving simulations. Future work could investigate the degree to which this is true over the tropics in GCMs.

As for Betts's rule (Rule 3), this has long been invoked as a mechanism behind the weakening of tropical circulations, particularly the Walker circulation, as in Vecchi and Soden (2007). But, the lack of accuracy of Betts's rule found here and in Schneider et al. (2010), as well as the fact that its prior validation in Held and Soden (2006) and Vecchi and Soden (2007) relied on a single GCM and used M_c evaluated at 500 hPa rather than cloud base, suggests that a firmer basis for reasoning about the large-scale circulation is required.

However, even with a firm grasp on how convective mass fluxes change with warming, as potentially provided by Rule 2, there are still overlooked and unanswered questions about how exactly such changes should affect the large-scale circulation. For instance, Held and Soden (2006) point out that changes in M_c do not necessarily determine changes in the large-scale circulation, as the latter is also profoundly influenced by the *spatial distribution* of convection. Indeed, in the unorganized RCE simulations analyzed here, there is no large-scale circulation at any SST, yet M_c decreases with warming according to Rule 2. These points notwithstanding, Vecchi and Soden (2007) argue that a weakening of M_c should lead to a proportional weakening of large-scale upward pressure velocities ω_{up}. This argument seems to assume that M_c is closely related to the large-scale gross mass flux $M_{\text{up}} \equiv -\frac{1}{g}\sigma_{\text{up}}\omega_{\text{up}}$ (Jenney et al., 2020, where σ_{up} is the fractional area occupied by ascending grid cells), *and* that σ_{up} does not change significantly with warming. Future work could test these assumptions and make the connection between M_c and other measures of the large-scale circulation (such as ω_{up}) more precise.

Finally, it is worth reflecting on the essential physics behind our rules. The physics behind Betts's Rule is straightforward enough: cloud-base moisture increases faster than column-integrated radiative cooling, so less mass flux is required. But are there analogous statements for Rules 1 and 2? The driving force there seems to be the increasing difference between $\Gamma(T)$ and Γ_d, particularly in the upper troposphere, as T_s increases (Figures A1a and A1b). What causes this? Even at a fixed upper-tropospheric isotherm T, $q_v^*(T)$ will still increase with T_s because the *pressure* and hence ambient air density are going down, even if the vapor pressure is not changing. This actually causes a quasi-exponential increase of $q_v^*(T)$ with T_s, even though the isotherm T is fixed (see detailed discussion in Romps, 2016). This increase of $q_v^*(T)$ then increases the latent heating of ascending parcels, leading to an increase in stability measures such as $1/\Gamma - 1/\Gamma_d$. Meanwhile, the $-\partial_T F$ factor in Equation 5 is T_s-invariant. Thus, Rule 2 (and also Rule 1, as a derivative of Rule 2) is again driven by a mismatch between the scalings of radiative cooling and moisture with T_s. This is reminiscent of Mapes's "two scale-heights" argument which contrasts the thermodynamic and radiative behaviors of water vapor (Mapes, 2001), but here applied to global warming rather than our base climate.

Appendix A: FV^3 Simulations

The atmospheric model used here is the non-hydrostatic version of GFDL's FV^3 (Finite-Volume Cubed-Sphere Dynamical Core, Harris & Lin, 2013; S.-J. Lin, 2004). The simulations analyzed here are very similar to those of Jeevanjee and Zhou (2022), so we describe some salient aspects of the simulation below, and refer the reader to Jeevanjee and Zhou (2022) for complete details.

We simulate doubly periodic radiative-convective equilibrium (RCE) over fixed sea surface temperatures of $T_s = 280$, 290, 300 and 310 K. Our particular FV^3 codebase is not equipped with interactive radiation, so radiative cooling must be otherwise parameterized. To emulate the T_s-dependence of interactive radiation, we parameterized it as a fit to the invariant divergence of radiative flux F found by Jeevanjee and Romps (2018):

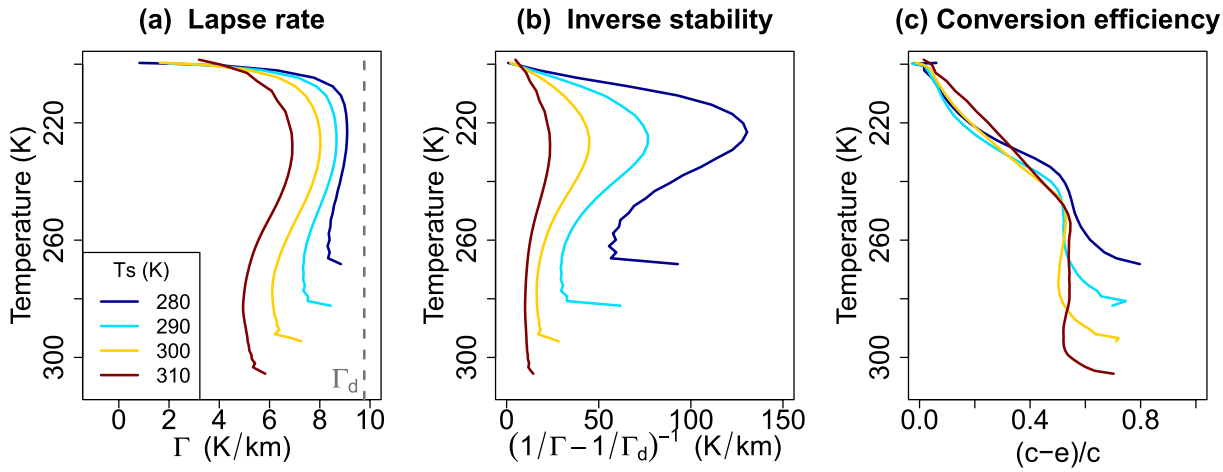

Figure A1. The lapse rate profiles $\Gamma(T)$ decrease with T_s and become more distant from the dry value (panel a), causing a marked decrease in the inverse stability parameter $(1/\Gamma - 1/\Gamma_d)^{-1}$ (panel b). Meanwhile, profiles of conversion efficiency are roughly T_s-invariant (panel c).

$$-\partial_T F = \left(0.025\,\mathrm{W/m^2/K^2}\right) \cdot \left(T - T_{tp}\right). \tag{A1}$$

Here the temperature derivative is a vertical derivative and $T_{tp} = 200$ K is the tropopause temperature. Above the tropopause temperatures are relaxed to T_{tp}, so the stratosphere is roughly isothermal. The invariance of $(-\partial_T F)(T)$ profiles with respect to T_s was shown on both theoretical grounds and with cloud-resolving simulations in Jeevanjee and Romps (2018), and also confirmed across cloud-resolving models in Stauffer and Wing (2022).

No boundary layer or sub-grid turbulence schemes are used. Microphysical transformations are performed with a warm-rain version of the GFDL microphysics scheme (Chen & Lin, 2013; Zhou et al., 2019), which in its default configuration models only water vapor q_v (kg/kg), cloud condensate, and rain, with the only transformations being condensation/evaporation of condensate and autoconversion of cloud condensate to rain (rain evaporation is disabled). The horizontal grid has 96 points in both x and y with a resolution of 1 km, and the 90-level vertical grid has a stretched grid spacing of 50 m near the surface up to 5,000 m near model top at 68 km. Each simulation ran for 120 days, with domain-mean statistics drawn from the last 5 days.

Actively convecting (updraft) grid cells are identified as having cloud condensate mixing ratios greater than 10^{-5} as well as vertical velocities $w > 0.7$ m/s, and convective mass fluxes are then defined at each level as $M \equiv \rho w_{up} \sigma_{up}$ (kg/m^2/s) where w_{up} is w conditionally averaged over updraft grid cells, and σ_{up} is the fractional area occupied by updraft grid cells (this σ_{up} should not be confused with the large-scale σ_{up} introduced in the conclusion). Cloud-base is defined as the lower-level maximum in cloud fraction, and the tropopause is defined as the lowest model within 0.5 K of $T_{tp} = 200$ K. Figure A1 shows three key diagnostics for the arguments presented in this paper: the lapse rate Γ, inverse stability parameter $(1/\Gamma - 1/\Gamma_d)^{-1}$, and conversion efficiency $\alpha = (c - e)/c$.

Appendix B: DAM Simulations

Our second set of cloud-resolving RCE simulations use Das Atmosphärische Modell (DAM, Romps, 2008), a fully compressible, non-hydrostatic cloud-resolving model, coupled to radiation via the comprehensive Rapid Radiative Transfer Model (RRTM, Mlawer et al., 1997). DAM employs the six-class Lin-Lord-Krueger microphysics scheme (Y.-L. Lin et al., 1983; Lord et al., 1984; Krueger et al., 1995), and in contrast to its original formulation in Romps (2008) employs no explicit sub-grid scale turbulence scheme, relying instead on "implicit LES" for sub-grid scale transport (Margolin et al., 2006).

These simulations ran on a square doubly periodic domain of horizontal dimension $L = 72$ km, with a horizontal grid spacing of $dx = 1$ km. The 76 level vertical grid has a spacing which stretches smoothly from 50 m below 1,000 m–250 m between 1,000 m and 5,000 m, and then to 500 m up to the model top at 30 km. We calculated surface heat and moisture fluxes using simple bulk aerodynamic formulae, and used a pre-industrial CO_2 concentration of 280 ppm with no ozone. Our SSTs are the same as for the FV^3 simulations, and all our DAM runs branched off the equilibrated runs described in Romps (2014) and were run for 60 days to iron out

any artifacts from changing the domain and resolution. All vertical profiles are time-mean and domain-mean, averaged over the last 5 days of each run. All diagnostics are constructed identically to their FV^3 counterparts, except the vertical velocity threshold for conditional sampling of convective mass flux is taken to be 1 m/s.

Appendix C: Betts's Original Rule

The original formulation of Betts's rule (A. Betts, 1998, his equation 1) was written in terms of surface evaporation, subsidence mass flux, and the difference in q_v between the boundary layer mean and the dry air sinking at boundary layer top. To write this in terms of the variables used here, we note the equivalence between surface evaporation and precipitation, and further assume that precipitation equals Q_{ft} (O'Gorman et al. 2012). We also invoke the equivalence between subsidence mass flux and convective mass flux [Equation 4 and Figure 3], and note that boundary layer mean q_v equals $q_v^*|_{LCL}$ since the LCL is (by definition) the level where boundary layer parcels become saturated. With these replacements, Betts's original rule becomes

$$Q_{ft} = L\left[M(1-\mathrm{RH})q_v^*\right]|_{LCL}. \tag{C1}$$

Unlike the version (Equation 6) appearing in Held and Soden (2006), this constraint can be derived without neglect of entrainment or non-unit PE, as follows. We again turn to the bulk-plume equations, for both in-plume and environmental moisture (e.g., Equations B6 and B7 of Romps, 2016):

$$\partial_z q_v^* = -\epsilon(1-\mathrm{RH})q_v^* - c/M$$

$$-\partial_z(\mathrm{RH}q_v^*) = \delta(1-\mathrm{RH})q_v^* + (1-\alpha)c/M$$

[note that our α equals $1-\alpha$ in Romps (2016)]. Adding these equations and noting that $\partial_z M = M(\epsilon-\delta)$, one can rewrite the result as

$$\alpha c = -\partial_z\left[(1-\mathrm{RH})Mq_v^*\right]. \tag{C2}$$

Integrating Equation 10 and invoking Equation C2 as well as the definition of vertically resolved $\alpha = (c-e)/c$ rather than PE yields

$$Q_{ft} = L\int_{z_{LCL}}^{z_{tp}} \alpha c\,dz = -L\int_{z_{LCL}}^{z_{tp}} \partial_z\left[(1-\mathrm{RH})Mq_v^*\right] = L\left[(1-\mathrm{RH})Mq_v^*\right]|_{LCL},$$

which is Equation C1.

It is remarkable that this version of Betts's rule does not neglect entrainment/detrainment or evaporation of condensate, unlike Equation 6. One must conclude that these effects are then entirely encapsulated in the value of $\mathrm{RH}|_{LCL}$. Given that the simplified form Equation 6 is not entirely robust, one must further conclude that $\mathrm{RH}|_{LCL}$ is relatively unconstrained and varies in our simulations. Indeed, both our FV^3 and DAM simulations show $\mathrm{RH}|_{LCL}$ increases of 0.2 over our SST range, yielding significant decreases in the $(1-\mathrm{RH})$ factor appearing in Equation C1.

Data Availability Statement

Data and analysis and visualization scripts used in generation of the figures in this paper are available at https://doi.org/10.5281/zenodo.6792098. Analysis and visualization was performed with the R computing language, available at https://www.r-project.org.

Acknowledgments
Linjiong Zhou assisted with configuring cloud-resolving simulations with FV^3 and developed the warm-rain option of the GFDL microphysics package. Jake Seeley, Zhihong Tan, Linjiong Zhou, and Andrew Williams provided valuable feedback on drafts of this work. Yi Ming provided encouragement and suggested the use of GFDL CM4 output. Huan Guo assisted with location of this output on the GFDL archive. Catherine Raphael produced the schematic in Figure 6. Two anonymous reviewers provided encouragement as well as useful critical feedback.

References

Betts, A. (1998). Climate-convection feedbacks: Some further issues. *Climatic Change*, *39*(1), 35–38. https://doi.org/10.1023/a:1005323805826

Betts, A. K., & Ridgway, W. (1989). Climatic equilibrium of the atmospheric convective boundary layer over a tropical ocean. *Journal of the Atmospheric Sciences*, *46*(17), 2621–2641. https://doi.org/10.1175/1520-0469(1989)046<2621:ceotac>2.0.co;2

Beydoun, H., Caldwell, P. M., Hannah, W. M., & Donahue, A. S. (2021). Dissecting anvil cloud response to sea surface warming. *Geophysical Research Letters*, *48*(15), 1–11. https://doi.org/10.1029/2021gl094049

Bony, S., Stevens, B., Coppin, D., Becker, T., Reed, K. A., Voigt, A., & Medeiros, B. (2016). Thermodynamic control of anvil cloud amount. *Proceedings of the National Academy of Sciences of the United States of America*, *113*(32), 8927–8932. https://doi.org/10.1073/pnas.1601472113

Chadwick, R., Boutle, I., & Martin, G. (2013). Spatial Patterns of Precipitation Change in CMIP5: Why the Rich Do Not Get Richer in the Tropics. *Journal of Climate*, *26*(11), 3803–3822. https://doi.org/10.1175/jcli-d-12-00543.1

Chen, J. H., & Lin, S. J. (2013). Seasonal predictions of tropical cyclones using a 25-km-resolution general circulation model. *Journal of Climate*, *26*(2), 380–398. https://doi.org/10.1175/jcli-d-12-00061.1

Cronin, T. W., & Wing, A. A. (2017). Clouds, circulation, and climate sensitivity in a radiative-convective equilibrium channel model. *Journal of Advances in Modeling Earth Systems*, *9*(8), 2883–2905. https://doi.org/10.1002/2017ms001111

Harris, L. M., & Lin, S.-J. (2013). A two-way nested global-regional dynamical core on the cubed-sphere grid. *Monthly Weather Review*, *141*(1), 283–306. https://doi.org/10.1175/mwr-d-11-00201.1

Hartmann, D. L., Blossey, P. N., & Dygert, B. D. (2019). Convection and climate: What have we learned from simple models and simplified settings? *Current Climate Change Reports*, *5*(3), 196–206. https://doi.org/10.1007/s40641-019-00136-9

Hartmann, D. L., & Larson, K. (2002). An important constraint on tropical cloud—Climate feedback. *Geophysical Research Letters*, *29*(20), 1951–12-4. https://doi.org/10.1029/2002gl015835

Held, I. M., Guo, H., Adcroft, A., Dunne, J. P., Horowitz, L. W., Krasting, J., et al. (2019). Structure and performance of GFDL's CM4.0 climate model. *Journal of Advances in Modeling Earth Systems*, *11*(11), 1–37. https://doi.org/10.1029/2019ms001829

Held, I. M., & Soden, B. J. (2006). Robust responses of the hydrological cycle to global warming. *Journal of Climate*, *19*(21), 5686–5699. https://doi.org/10.1175/jcli3990.1

Ito, M., & Masunaga, H. (2022). Process-level assessment of the Iris effect over tropical oceans. *Geophysical Research Letters*, *49*(7), 1–9. https://doi.org/10.1029/2022gl097997

Jeevanjee, N., Hassanzadeh, P., Hill, S., & Sheshadri, A. (2017). A perspective on climate model hierarchies. *Journal of Advances in Modeling Earth Systems*, *9*(4), 1760–1771. https://doi.org/10.1002/2017ms001038

Jeevanjee, N., & Romps, D. M. (2018). Mean precipitation change from a deepening troposphere. *Proceedings of the National Academy of Sciences of United States of America*, *115*(45), 11465–11470. https://doi.org/10.1073/pnas.1720683115

Jeevanjee, N., & Zhou, L. (2022). On the resolution-dependence of anvil cloud fraction and precipitation efficiency in radiative-convective equilibrium. *Journal of Advances in Modeling Earth Systems*, *14*(3). https://doi.org/10.1029/2021ms002759

Jenney, A. M., Randall, D. A., & Branson, M. D. (2020). Understanding the response of tropical ascent to warming using an energy balance framework. *Journal of Advances in Modeling Earth Systems*, *12*(6). https://doi.org/10.1029/2020ms002056

Knutson, T. R., Manabe, S., Mechoso, C. R., & Ghil, M. (1995). Simulation of the tropical Pacific climate with a coupled ocean-atmosphere general circulation model. Part I: The seasonal cycle. *Journal of Climate*, *8*(5), 1178–1198. https://doi.org/10.1175/1520-0442(1995)008<1178:sottpc>2.0.co;2

Krueger, S. K., Fu, Q., Liou, K. N., & Chin, H.-N. S. (1995). Improvements of an ice-phase microphysics parameterization for use in numerical simulations of tropical convection. *Journal of Applied Meteorology*, *34*(1), 281–287. https://doi.org/10.1175/1520-0450-34.1.281

Lin, S.-J. (2004). A 'vertically Lagrangian' finite-volume dynamical core for global models. *Monthly Weather Review*, *132*(10), 2293–2307. https://doi.org/10.1175/1520-0493(2004)132<2293:avlfdc>2.0.co;2

Lin, Y.-L., Farley, R. D., & Orville, H. D. (1983). Bulk parameterization of the snow field in a cloud model. *Journal of Climate and Applied Meteorology*, *22*(6), 1065–1092. https://doi.org/10.1175/1520-0450(1983)022<1065:bpotsf>2.0.co;2

Lord, S. J., Willoughby, H. E., & Piotrowicz, J. M. (1984). Role of a parameterized ice-phase microphysics in an axisymmetric, non hydrostatic tropical cyclone model. *Journal of the Atmospheric Sciences*, *41*(19), 2836–2848. https://doi.org/10.1175/1520-0469(1984)041<2836:roapip>2.0.co;2

Lutsko, N., Sherwood, S. C., & Zhao, M. (2021). *Precipitation Efficiency and Climate Sensitivity (Invited Chapter for the AGU Geophysical Monograph Series "Clouds and Climate")*. https://doi.org/10.1002/essoar.10507822.1

Mapes, B. E. (2001). Water's two scale heights: The moist adiabat and the radiative troposphere. *Quarterly Journal of the Royal Meteorological Society*, *127*, 2353–2366. https://doi.org/10.1002/qj.49712757708

Margolin, L. G., Rider, W. J., & Grinstein, F. F. (2006). Modeling turbulent flow with implicit LES. *Journal of Turbulence*, *7*, N15. https://doi.org/10.1080/14685240500331595

Mlawer, E. J., Taubman, S. J., Brown, P. D., Iacono, M. J., & Clough, S. A. (1997). Radiative transfer for inhomogeneous atmospheres: RRTM, a validated correlated-k model for the longwave. *Journal of Geophysical Research*, *102*(D14), 16663–16682. https://doi.org/10.1029/97jd00237

Morrison, H., van Lier-Walqui, M., Fridlind, A. M., Grabowski, W. W., Harrington, J. Y., Hoose, C., et al. (2020). Confronting the challenge of modeling cloud and precipitation microphysics. *Journal of Advances in Modeling Earth Systems*, *12*(8). https://doi.org/10.1029/2019ms001689

O'Gorman, P. A., Allan, R. P., Byrne, M. P., & Previdi, M. (2012). Energetic Constraints on Precipitation Under Climate Change. *Surveys in Geophysics*, *33*(3–4), 585–608. https://doi.org/10.1007/s10712-011-9159-6

Ohno, T., Noda, A. T., & Satoh, M. (2020). Notes and correspondence impacts of sub-grid ice cloud physics in a turbulence scheme on high clouds and their response to global warming. *Journal of the Meteorological Society of Japan*, *98*(5), 1069–1081. https://doi.org/10.2151/jmsj.2020-054

Ohno, T., Noda, A. T., Seiki, T., & Satoh, M. (2021). Importance of pressure changes in high cloud area feedback due to global warming. *Geophysical Research Letters*, *48*(18). https://doi.org/10.1029/2021gl093646

Ohno, T., & Satoh, M. (2018). Roles of cloud microphysics on cloud responses to sea surface temperatures in radiative-convective equilibrium experiments using a high-resolution global nonhydrostatic model. *Journal of Advances in Modeling Earth Systems*, *10*(8), 1970–1989. https://doi.org/10.1029/2018ms001386

Romps, D. M. (2008). The dry-entropy budget of a moist atmosphere. *Journal of the Atmospheric Sciences*, *65*(12), 3779–3799. https://doi.org/10.1175/2008jas2679.1

Romps, D. M. (2014). An analytical model for tropical relative humidity. *Journal of Climate*, *27*(19), 7432–7449. https://doi.org/10.1175/jcli-d-14-00255.1

Romps, D. M. (2016). Clausius-clapeyron scaling of CAPE from analytical solutions to RCE. *Journal of the Atmospheric Sciences*, *73*(9), 3719–3737. https://doi.org/10.1175/jas-d-15-0327.1

Saint-Lu, M., Bony, S., & Dufresne, J. L. (2020). Observational evidence for a stability Iris effect in the tropics. *Geophysical Research Letters*, *47*(14). https://doi.org/10.1029/2020gl089059

Saint-Lu, M., Bony, S., & Dufresne, J.-L. (2022). Clear-sky control of anvils in response to increased CO_2 or surface warming or volcanic eruptions. *Npj Climate and Atmospheric Science*, *5*(1). https://doi.org/10.1038/s41612-022-00304-z

Schneider, T., O'Gorman, P., & Levine, X. (2010). Water vapor and the dynamics of climate changes. *Reviews of Geophysics*, *48*(48), 1–22. https://doi.org/10.1029/2009rg000302

Seeley, J. T., Jeevanjee, N., Langhans, W., & Romps, D. M. (2019). Formation of tropical anvil clouds by slow evaporation. *Geophysical Research Letters*, *46*(1), 492–501. https://doi.org/10.1029/2018gl080747

Sherwood, S. C., Webb, M. J., Annan, J. D., Armour, K. C., Forster, P. M., Hargreaves, J. C., et al. (2020). An assessment of earth's climate sensitivity using multiple lines of evidence. *Reviews of Geophysics*, *58*(4), 1–92. https://doi.org/10.1029/2019rg000678

Singh, M. S., & O'Gorman, P. A. (2013). Influence of entrainment on the thermal stratification in simulations of radiative-convective equilibrium. *Geophysical Research Letters*, *40*(16), 4398–4403. https://doi.org/10.1002/grl.50796

Singh, M. S., & O'Gorman, P. A. (2015). Increases in moist-convective updraught velocities with warming in radiative-convective equilibrium. *Quarterly Journal of the Royal Meteorological Society*, *141*(692), 2828–2838. https://doi.org/10.1002/qj.2567

Stauffer, C. L., & Wing, A. A. (2022). Properties, changes, and controls of deep-convecting clouds in radiative-convective equilibrium. *Journal of Advances in Modeling Earth Systems*, *14*(6). https://doi.org/10.1029/2021ms002917

Tsushima, Y., Iga, S. I., Tomita, H., Satoh, M., Noda, A. T., & Webb, M. J. (2014). High cloud increase in a perturbed SST experiment with a global nonhydrostatic model including explicit convective processes. *Journal of Advances in Modeling Earth Systems*, *6*(3), 571–585. https://doi.org/10.1002/2013ms000301

Vecchi, G. A., & Soden, B. J. (2007). Global warming and the weakening of the tropical circulation. *Journal of Climate*, *20*(17), 4316–4340. https://doi.org/10.1175/jcli4258.1

Wing, A. A., Stauffer, C. L., Becker, T., Reed, K. A., Ahn, M., Arnold, N. P., et al. (2020). Clouds and convective self-aggregation in a multi-model ensemble of radiative-convective equilibrium simulations. *Journal of Advances in Modeling Earth Systems*, *12*(9), 1–72. https://doi.org/10.1029/2020ms002138

Zhao, M., Golaz, J.-C., Held, I. M., Guo, H., Balaji, V., Benson, R., et al. (2018). The GFDL global atmosphere and land model AM4.0/LM4.0: 2. Model description, sensitivity studies, and tuning strategies. *Journal of Advances in Modeling Earth Systems*, *10*(3), 735–769. https://doi.org/10.1002/2017ms001209

Zhou, L., Lin, S. J., Chen, J. H., Harris, L. M., Chen, X., & Rees, S. L. (2019). Toward convective-scale prediction within the next generation global prediction system. *Bulletin of the American Meteorological Society*, *100*(7), 1225–1243. https://doi.org/10.1175/bams-d-17-0246.1

Erratum

The originally published version of this article contained a few typographical errors. In the sixth line of the fourth paragraph of Section 2, the phrase "the mean anvil" has been removed. In the fifth and eighth lines of the fourth paragraph of Section 3, the word "increases" should be "decreases." In addition, in the caption to Figure A1, the word "increase" should be "decrease." The errors have been corrected, and this may be considered the authoritative version of record.